

Using Sentinel-2 time series to detect slope movement before the Jinsha River landslide

Abstract Detecting slope movement before landslides occur in mountain regions is crucial for disaster reduction. In October 2018, a gigantic landslide occurred on the Jinsha River, causing dammed-lake breach flood 500 km downstream. In this work, we used 25 Sentinel-2 images from November 2015 to August 2018 to explore the capability of this high temporal resolution optical images in detecting slope movement before the Jinsha River landslide. Normalized difference vegetation index (NDVI) was calculated to composite temporal profiles using all Sentinel-2 images. With this NDVI time series, unsupervised K-means classifier was applied to initially classify the study area and find the best thresholds for automatically extracting landslide scars in the image series. These extracted landslide scars were validated using interpreted results from two high spatial resolution images of similar dates in 2015 (user's accuracy 89.7%, producer's accuracy 83.6%) and 2018 (user's accuracy 90.8%, producer's accuracy 74.9%). After validation, extracted landslide scars of different years were counted and displayed in an RGB composite image to highlight slope movement. In addition, monotonous decrease/increase of NDVI was also observed, indicating continuous expansion of landslide scarps and movement of landslide head along the slope on the landslide surface. This work demonstrated the capability of Sentinel-2 time series images to capture slope movement with short revisit time at low cost. By incorporating other environmental information (such as elevation), this proposed method has the potential to consistently map pre-landslide slope movements over a large region.

Keywords Pre-landslide · Slope movement detection · Sentinel-2 · Optical remote sensing

Introduction

On 10 October 2018, a massive landslide occurred on the right bank of the Jinsha River, forming a dammed lake with the volume of $\sim 2 \times 10^8 \text{ m}^3$ (Fan et al. 2019). Despite this landslide is located in a remote and sparsely populated region, its impact is profound. Uprising water inundated upstream Boluo town in the Tibet Autonomous Region and subsequent flood released from the dam caused millions of dollar loss in downstream area as far as 500 km away (Xinhua 2018a).

Such major landslides could also occur in other mountain regions of the world, which could have either direct or indirect consequences on human society (Fan et al. 2017; Igwe 2018). Luckily, there always seems to be a slope movement before their sudden failure (Wasowski and Bovenga 2014). Therefore, detecting pre-landslide slope movement is crucially important for disaster mitigation.

Previous works on detecting slope movement before landslides have mostly been focused on SAR techniques (Intrieri et al. 2018; Lu et al. 2012; Tomás et al. 2016) and high spatial

resolution optical remote sensing (Lacroix et al. 2015; Stumpf et al. 2017). Although SAR techniques have the capability to detect millimeter scale surface deformation, they are effective for minor slope displacements and are often affected by unfavorable conditions, such as dense vegetation and steep topography (Intrieri et al. 2018; Wasowski and Bovenga 2014; Wright 2002). Unfortunately, many catastrophic landslides occur in vegetation-covered remote areas with very rough topography, and applying SAR techniques to investigate potential pre-landslide slope movement in a large region have been difficult (Wasowski and Bovenga 2014). Other works monitoring slope displacement on landslide surface use very high spatial resolution images (Lacroix et al. 2015; Stumpf et al. 2017). These images require strict co-registrations and rely on non-vegetation ground features to track slope movement. In addition, they cover a limited area and are very expensive to use for frequent observation in large regions.

Detecting pre-landslide slope displacement using openly accessible, moderate to high spatial resolution optical satellite images such as Landsat and Sentinel-2 datasets has been less studied. These datasets have short regular observation intervals for the same location. Sentinel-2 is a European Space Agency satellite constellation to monitor the land environment on the earth's surface. It has two identical polar-orbiting satellites: Sentinel-2A and 2B. Sentinel-2A was launched on 23 June 2015 and Sentinel-2B was launched on 7 March 2017. Both Sentinel-2 satellites have a spatial resolution of 10 m in near-infrared, red, green, and blue bands. The Sentinel-2 constellation has a revisit time of 5-day at the Equator and is freely distributed to the public. An advantage of these optical remote sensing image is that it has more spectral information and is very sensitive to capture vegetation disturbance caused by landslide activity (Yang et al. 2013). Recently, the study of Sentinel-2 in natural hazards (such as fault detection, floods, wildfire) has been commenced (Notti et al. 2018; Sanchez et al. 2018; Elhag and Alshamsi 2019), but its potential use in regional landslide hazard studies has been less explored (Lacroix et al. 2018). In one recent work, Lacroix et al. (2018) used Cosi-Corr technique with Sentinel-2 images to detect precursors before a landslide occurs in the French Alps. The Cosi-Corr technique compares two images to produce ground deformation. It requires both images to have a short temporal interval to be correlated, and large displacements occur between both images (Leprince et al. 2007). Uncertainties increase significantly with the increase of temporal interval, and the Cosi-Corr method have problems in detecting slow movement over long periods.

In this work, we aim to develop a simple but effective method to use time series of all available Sentinel-2 images to detect slope movement over a long term. We took the Jinsha River landslide as an example to attract attention from the landslide community to fully exploit this lately available Sentinel-2 data.

Study area

On 10 October 2018, a major landslide occurred on the west bank of the Jinsha River (31°4′58″ N, 98°42′19″ E, 3300 m a.s.l., Fig. 1). This section of the Jinsha River is a natural boundary between Sichuan Province and the Tibet Autonomous Region. The elevation of the landslide crown is 3700 m and the Minjiang River at the landslide foot is 2900 m. Initiated on the west bank, landslide materials rushed downslope and blocked the Jinsha River twice. Interpretation of post-landslide Sentinel-2 images (Fig. 2) indicates that the deposited materials on the opposite east slope of the river reached an elevation of 3000 m. The volume of the Jinsha River landslide was estimated to be $\sim 2.4 \times 10^7 \text{ m}^3$ and it formed a dammed lake of $\sim 2 \times 10^8 \text{ m}^3$ (Fan et al. 2019). Rising water inundated Boluo town 15 km upstream, and the subsequent dam breached flood destroyed downstream houses as far as Lijiang city in Yunnan Province, which is 500 km away (Xinhua 2018a).

The total area of the studied region is 5.88 km² as shown in Fig. 2. It is located in the upper stream of the Yangtze River (also known as the Jinsha River in this section). The study area is tectonically active and is a transition zone from the Tibetan plateau (mean elevation > 4000 m) to the Sichuan Basin (mean elevation ~ 500 m). Valleys are deeply incised by large rivers. Tension cracks on the slope are clearly visible in a Google Earth image in March 2011. The triggering reason for the landslide in October 2018 is unknown, and there is no report on the direct cause of this landslide at the moment. It is clear that this landslide is a progressive one and probably existed for a few decades (Xu et al. 2018). This area has a few earthquakes since 2000 (Fig. 1b, data source: USGS), but no earthquake was recorded since 2016.

Earthquake should not be responsible for the final failure of the landslide.

This study area has a monsoon climate and the annual precipitation is 641.2 mm (30 years' average from 1989 to 2018) and >75% precipitation occur between June and September each year (Fig. 3a). Probably influenced by precipitation, the slope moves down gradually for a few decades before its complete failure (Xu et al. 2018). By the time the landslide occurred, accumulated precipitation in 2018 of the study area reached 718 mm, significantly higher than previous years (2015–2017, Fig. 3b). Although this amount of precipitation is not the highest in history (Fig. 3c), considering the progressive movement of slope this amount of precipitation could be more effective in leading to the final failure of the slope on 10 October 2018.

Although roads can be seen on the landslide surface from historical Google Earth images, this region is sparsely populated and human activity is unlikely the reason for the failure of this landslide. Except for a few sections of roads on the top of the landslide, there are no signs of human undercutting or other interventions. In addition, local geological conditions may also contribute to this landslide. The landslide head is composed of fractured serpentine rock bordering with gneiss beneath. It is reported that an active fault cut through the ridge of the slope (Xu et al. 2018). It is possible that this deeply incised slope was initially undermined by historical tectonic activities. Since then, strains were accumulated with multi-year precipitation and the crown deformed with tension cracks enlarged year by year. Near the critical moment, shear stress was overwhelmed with more accumulated precipitation in 2018 than in previous years.

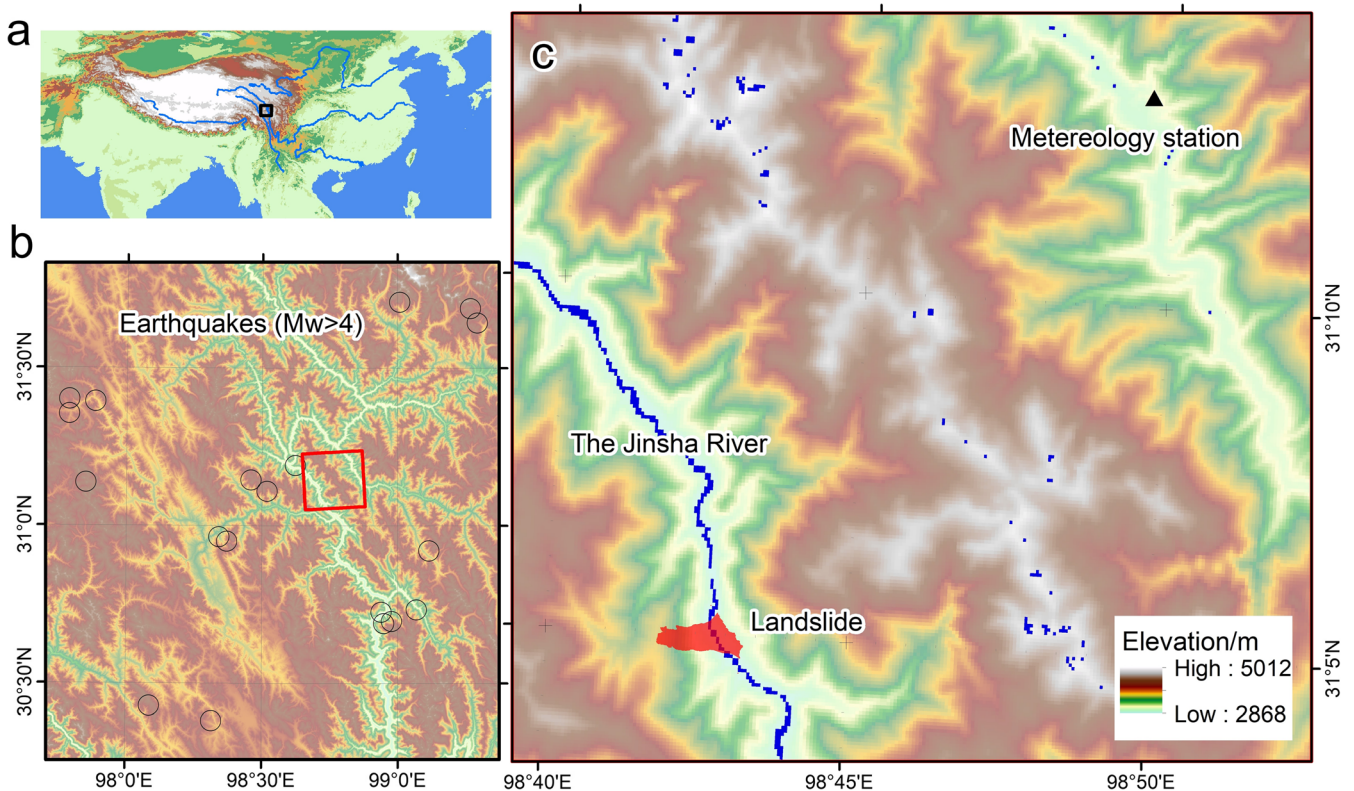


Fig. 1 Location and topography of the study area. This study area is in east Tibetan Plateau (a). There are some historical earthquakes with $M_w > 4.0$ since 2000 (b). The nearest meteorological station is 18 km away from the landslide (c)

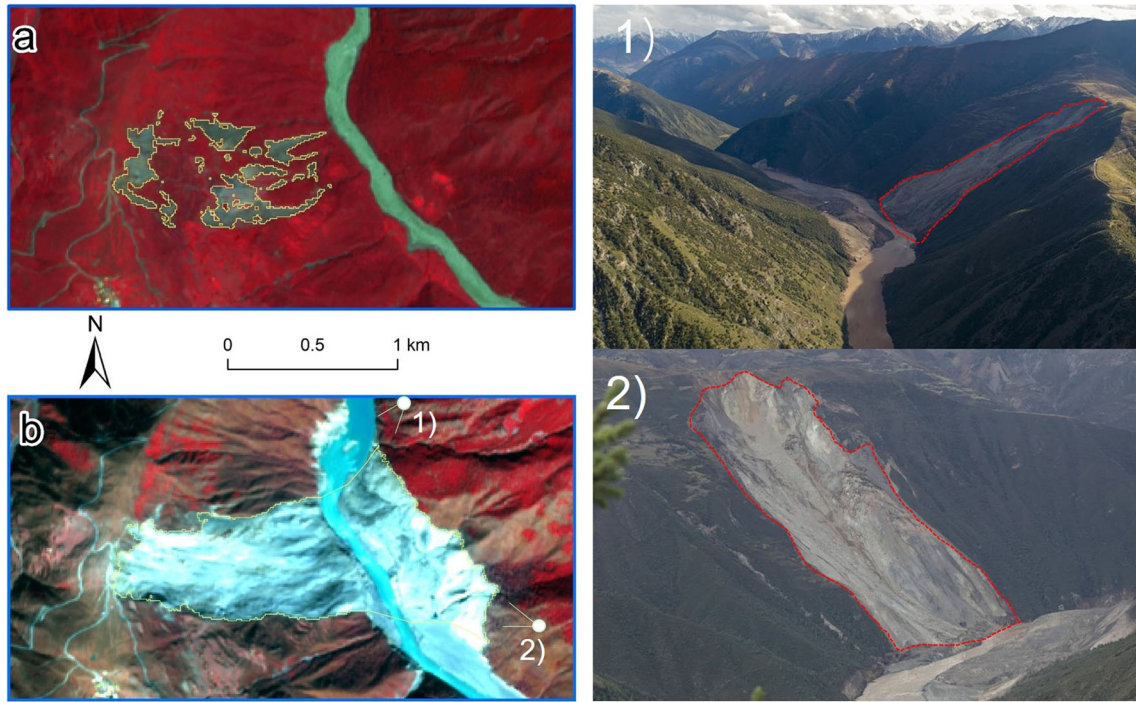


Fig. 2 Sentinel-2 images and photos of the landslide. False color composite images before (on 4 August 2017) (a) and after (2 November 2018) the landslide (b). In map (b) are two directions the photos of 1 and 2 were taken. Online source: photo 1 (Xinhua 2018b) and photo 2 (Baidu 2018)

Data

The Sentinel-2 constellation have much higher spatial resolution (10 m multi-spectral) and more frequent revisit interval (5-day) than previously openly accessed data (such as the 16-day interval 30-m Landsat images) in the world. Launched recently, the Sentinel-2 time series data used in this area has long and irregular time intervals. In this work, we downloaded 25 images of Sentinel-2 Level-1C products from November 13, 2015 to August 9, 2018. Of these Sentinel-2 images, there are three images in 2015, five images in 2016, eleven in 2017 and six in 2018 (Table 1). At this level, these multi-temporal images were registered better than 0.3 pixels (Gascon et al. 2017). These images cover an area of 5.88 km² (1.76 km × 3.34 km), totally include the landslide and are cloud free at least for the landslide surface. To validate Sentinel-2 results, a 2 m resolution Ziyuan-3 image on 13 November 2015 and a 1 m resolution Gaofen-2 image on 28 February 2018 were used.

Method

This work used time series optical images of Sentinel-2 to detect slope movement before a major landslide occur. To detect slope movement, three procedures were implemented. Firstly, NDVI time series was composed and unsupervised classification was applied to classify potential landslide scars. Secondly, NDVI thresholds were determined to extract landslide scars for all Sentinel-2 images. Detected landslide scars from two Sentinel-2 images were validated using results interpreted from higher spatial resolution images. Finally, slope movement was analyzed using detected landslide scars and NDVI time series.

Classify NDVI time series

Normalized Difference Vegetation Index (NDVI) is commonly used in optical images to map landslide inventories (Yang et al. 2017; Zhang et al. 2018). By using NDVI in landslide interpretation, the influence of shadows in mountain region can be minimized

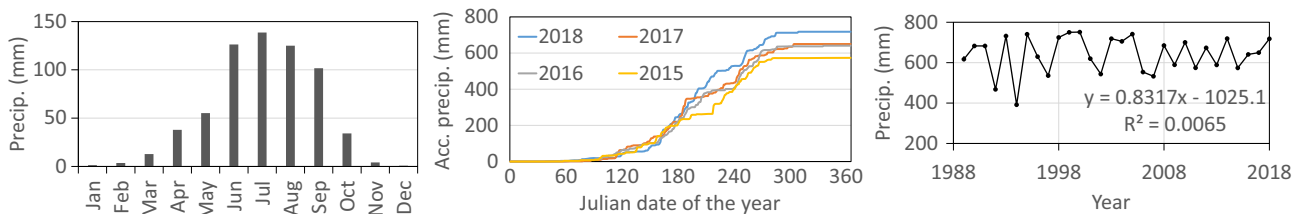


Fig. 3 Monthly average precipitation (1989–2018) of the nearest meteorological station (a), accumulated daily precipitation in 2015–2018 (b), and 30 years' annual precipitation from 1989 to 2018 (c)

Table 1 List of Sentinel-2 images used in this work (asterisks in brackets indicate clouds in the image)

Seasons	2018	2017	2016	2015	Date buffer
Spring		16 Jan			
		26 Jan			
	11 Apr(*)	5 Feb			
	5 Jun	16 May	11 May		24
Summer	10 Jun				
	25 Jun(*)	15 Jul			
	25 Jul	30 Jul(*)	30 Jul(*)		5
	9 Aug(*)	4 Aug			
Winter		24 Aug			
		8 Sep(*)			
		18 Oct	7 Nov	13 Nov	16
		28 Oct	7 Dec	23 Nov	
			27 Dec	23 Dec	

(Fiorucci et al. 2018). For all Sentinel-2 images in this work, we calculated the NDVI,

$$NDVI = \frac{\rho_{nir} - \rho_{red}}{\rho_{nir} + \rho_{red}}, \quad (1)$$

where, ρ_{nir} , ρ_{red} are reflectance of the near infrared and red bands. Then, these NDVI images were stacked to form NDVI time series with 25 layers in a chronological order using the Layer Stack module in ENVI software version 5.1.

Unsupervised K-means classification method in ENVI was used to classify the Sentinel-2 derived NDVI time series. Before performing the K-means classifier, the number of classes must be assigned. During classification, pixels cluster into this assigned number of classes in the 25-dimension feature space (25 images) by minimizing intra-class feature distances and maximizing inter-classes distances (Zhu and Helmer 2018). Because we only use the K-means unsupervised classifier to get a preliminary classification map, default parameters in the ENVI K-means module were used to perform the classification (e.g., class number is set to five).

Extract and validate landslide scars

In this work, landslide scars are defined as bare soil/rocks exposed by slope movement before the landslide occurred. They can be slope fissures or lose deposits released from the damaged slope, which is different from surrounding vegetation. Based on the K-means classification results, the class with potential landslide scars was selected. For every NDVI image, mean NDVI was calculated by averaging NDVI values in that class of potential landslide scars. The mean NDVIs were used as thresholds to extract landslide scars in each image.

To validate detected landslide scars, we collected two high spatial resolution images that temporally match the Sentinel-2 images. The first one is a 2 m resolution Ziyuan-3 image taken on 13 November 2015, and the second is a 1 m Gaofen-2 image taken on 28 February 2018. Landslide scars on Ziyuan-3 and

Gaofen-2 images were manually interpreted with the assistance of higher resolution images in Google Earth and are used as reference maps to validate automatically extracted landslide scars in Sentinel-2 images. Landslide scars in two Sentinel-2 images on 13 November 2015 and on 11 April 2018 were validated because they have the least date difference with those higher resolution images (Ziyuan-3 and Gaofen-2).

Detect slope movement

To detect slope movement, we analyzed both landslide scars and NDVI time series. Using the landslide scar thresholds, we extracted landslide scars on every Sentinel-2 image. We grouped landslide scar images into three periods: 2015–2016, 2017, and 2018 and counted the times of every pixel detected as landslide scar in that period. The counts were normalized to the range of 0–1 divided by their total image number in their corresponding periods. Then, we get three images of the scar count percentage and displayed the three images in an RGB composite to illustrate slope movement.

Based on the RGB composite, NDVI time series on the landslide was further analyzed. To use vegetation dynamics to indicate slope movement before the landslide occurred, only maximum NDVI in these 25 images larger than 0.3 were considered and a rule was set:

$$\text{if } \max(NDVI_{2016}) > \max(NDVI_{2017}) > \max(NDVI_{2018}) \quad (2)$$

$$\text{or } \max(NDVI_{2016}) < \max(NDVI_{2017}) < \max(NDVI_{2018}) \quad (3)$$

$$\text{then, } NDVI_{change} = \max(NDVI_{2016}) - \max(NDVI_{2018}) \quad (4)$$

where, $NDVI_{2016}$, $NDVI_{2017}$, and $NDVI_{2018}$ are NDVI values of a specific pixel in 2016, 2017, and 2018. By using Eqs. (2–4), the difference in annual maximum NDVI between 2016 and 2018 was calculated for pixels with monotonous decrease/increase changes.

For example, monotonous decrease in annual maximum NDVI in Eq. (3) can be used to indicate depressed slope vegetation by continuous landslide scarp expansion, whereas monotonous increase in Eq. (4) can be used to show landslide head with vegetation moves downslope, replacing non-vegetation landslide toes at the given location.

We also quantified NDVI changes in spring, summer, and winter seasons to indicate slope movement of different times. The rules were similar but we only considered NDVI series that are not landslide scars using extracted thresholds. Monotonous NDVI changes in 11 May 2016, 16 May 2017, and 5 July 2018 were calculated to indicate slope movement in springs of 2016–2018. The maximum date difference in these three images is 24 days (date buffer in Table 1). Monotonous NDVI changes in 30 July 2016, 30 July 2017, and 25 July 2018 were calculated to indicate slope movement in summers of 2016–2018 with date buffer of 5 days, and NDVI changes in 13 November 2015, 7 November 2016, and 28 October 2017 were calculated for winters of 2015–2017 (date buffer of 16 days).

Results

NDVI time series classification

Although class number was set to five in the K-means unsupervised classification model, the classification image around the landslide has three major classes: consistent bare land surface with no vegetation (Class 1, red pixels in Fig. 4), circumambient class (Class 2, green pixels in Fig. 4), and consistent vegetation class (Class 3, blue pixels in Fig. 4). Class 1 has consisted of ground features with consistently no vegetation cover, including landslide scars (shown as upper major scarp and lower toes in Fig. 4), roads, and the Jinsha River. In this class, roads and river are linear features, whereas landslide scars are irregular and located on the same slope. Class 3 is ground features with consistent vegetation

cover. Class 3 on the landslide has two part: the upper part is the unbroken landslide head and the lower part is the intact slope below the landslide toe. Bordered by Class 1 and Class 3, Class 2 is a transition zone between these two classes, possibly denoting unstable vegetation signals in this zone. Using sub-meter high spatial resolution from Google Earth, we found Class 4 and Class 5 are probably open and closed canopy evergreen coniferous forests, respectively. Therefore, these two classes are discarded for further analysis.

Landslide scar extraction and validation

From unsupervised classification, we can see that Class 1 are landslide scars of consistently no vegetation. To automatically extract bare landslide scars in each Sentinel-2 image, NDVI thresholds were determined by using the mean NDVI of Class 1 in each image. Figure 5 shows thresholds for the 25 Sentinel-2 images used in this work in chronological order. From this result, we can see that NDVI of the landslide scars remains in low values in the study period (< 0.3). Both seasonality and thin clouds can influence NDVI values on the landslide scars. NDVI values are higher in summer and lower in winter. This is because the spatial resolution of Sentinel-2 image is 10 m, and pixels at the landslide scar may be mixed by neighboring vegetation. It is also possible that herbaceous vegetation may grow in summer seasons during transient stable periods. By visually examining Sentinel-2 images, we found the high NDVI thresholds on 8 September 2017 and 30 July 2016 were caused by thin clouds on the landslide scar.

By comparison, we found the spatial patterns of the reference, and the detected scars are very similar (Fig. 6a, b). Careful examination reveals that there are larger omission errors than commission errors (Fig. 6 and Table 2). This means that the Sentinel-2 images perform well in identifying landslide scars (89.7% in 2015 and 90.8% in 2018) but at the cost of missing some true ones (missed 16.4% in 2015 and 25.1% in 2018). Although the spatial

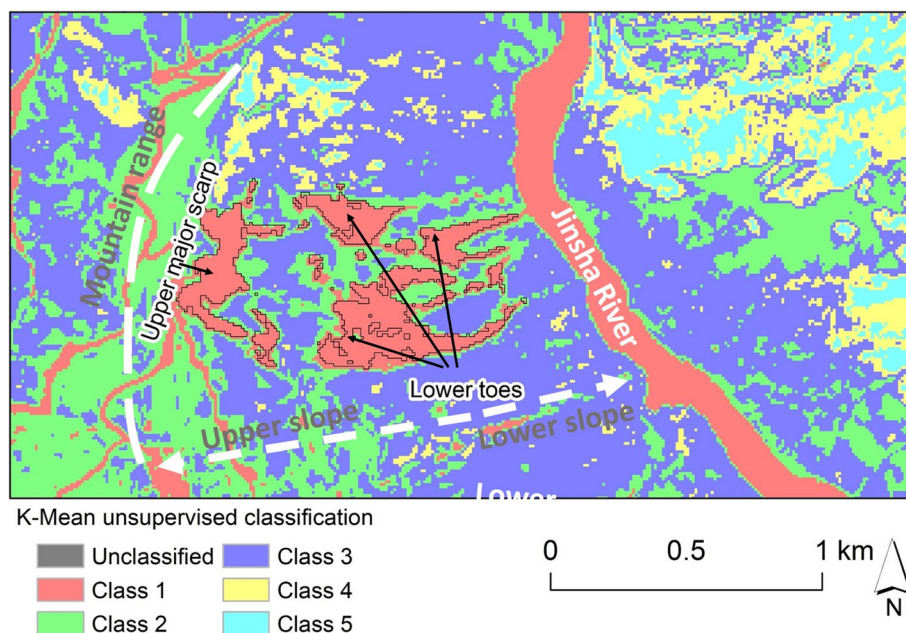


Fig. 4 K-means unsupervised classification of the NDVI time series surrounding the Jinsha landslide

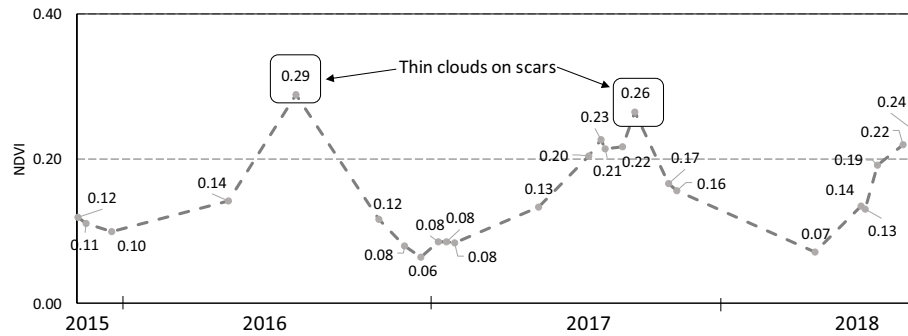


Fig. 5 Automatically determined NDVI thresholds to extract landslide scars for each Sentinel-2 image used in this work

resolution of Gaofen-2 image (1 m) in 2018 is better than the Ziyuan-3 image (2 m) in 2015, the producer's accuracies in 2015 (83.6%) are much higher than that of 2018 (74.9%). This is because the Sentinel-2 image in 2015 have the same date with the Ziyuan-3 image, whereas the date difference between the 2018 Sentinel-2 (11 April) and Gaofen-2 (28 February) images are 42 days. It is possible that the landslide surface experienced some changes during that time. Compared with the result in 2015, larger omission errors occurred in the extracted result of 2018. These omissions mainly occur on the uppermost part of the landslide, whereas the boundary of the lower part is accurate. It is likely that those undetected part is not active at that moment, highlighting sensitivity of the sensors onboard Sentinel-2 in detecting vegetation signals.

Slope movement indicated by landslide scar counts

To display slope movement, we made an RGB composite image by putting the scar count percentage of 2018 in the red channel, the resulting image of 2017 in green and 2015–2016 in blue channel

(Fig. 7). Because this RGB composite is composed in the order of 2018 to 2015 in the RGB channels, warm colors (e.g., red) indicate increasing counts of labeled landslide scar for the pixel from 2015 to 2018. In contrast, cold colors (e.g., blue) indicate decreasing counts of landslide scars from 2015 to 2018. Warm colors in the RGB composite image mean the landslide scar in 2018 are newly emerged features and cold colors mean the previously existed landslide scar disappeared. White colored pixels indicate pixels persistently labeled as landslide scars (notice that water can be easily excluded). Gray-colored pixels are never labeled as landslide scar in all periods.

From the RGB composite image, we can see colors on the landslide are distinctly different from the surrounding ground features. To analyze slope movement, we delineated two profiles, P1 and P2, along the slope from the mountain range to the Jinsha River valley. Along P1, there are warm color pixels on the lower boundary of the upper major scarp and cold color pixels on the upper boundary of the lower toes. This indicates that the lower

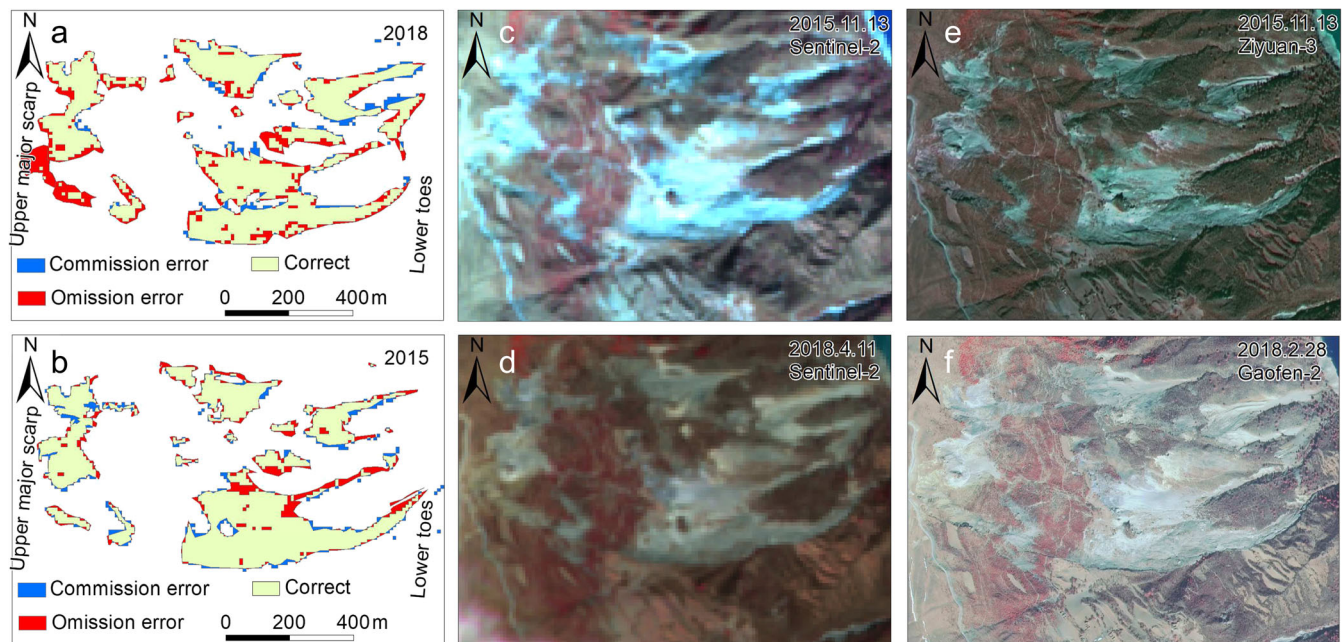


Fig. 6 Validation of the landslide scars (a and b) extracted from two Sentinel-2 images on 13 November 2015 (c) and 11 April 2018 (d) using a 2 m resolution Ziyuan-3 image (on 13 November 2015, (e)) and a 1 m resolution Gaofen-2 image (on 28 February 2018 (f))

Table 2 Accuracy of landslide scars mapped from two Sentinel-2 images

	Correct (m ²)	Omission error (m ²)	Commission error (m ²)	User's accuracy	Producer's accuracy
2015	179,119.7	35,128.7	20,623.6	89.7%	83.6%
2018	189,183.0	19,113.0	63,553.8	90.8%	74.9%

boundary of the upper major scarp enlarged and the upper boundary of the landslide toes retreated. It is probably because the slope between the upper major scarp and the lower toes slides down.

We also delineated another profile, P2, to analyze slope movement. Compared with P1, both the red-colored pixels in the lower boundary of the upper major scarp and blue colored pixels in the upper boundary of the lower toes are fewer, indicating this part of the slope has smaller slope displacements compared to P1. However, there are many red pixels in the lower boundary of the lower toes. This may not be caused by slope displacement, but rather caused by the release of debris from the broken of the slope, indicating that the lower part of the slope is very active before the landslide occurred.

Slope movement indicated by NDVI changes

We further analyzed NDVI time series for different colors shown in the RGB composite image (Fig. 8). Pixels in white color (Fig. 7) have consistently lower NDVI values compared with the other types, and they are major scarps and toes of the landslide without any vegetation throughout the study period. Point 1 in Fig. 7 have cold blue color and its NDVI time series is displayed as the typical increasing NDVI (Fig. 8). This kind of pixels has cold colors and is mainly located on the upper boundary of the lower toes. Point 3 in Fig. 8 have warm color, and its time series is displayed as typical decreasing NDVI (Fig. 8). This type of pixels is at the lower boundary of the upper major scarp and lower boundary of the

lower toes. Along the profile P1 (Fig. 7), red pixels at the lower part of the upper major scarp and the blue pixels at the upper part of the lower toes clearly indicate that the slope between them (i.e., the landslide head) moved down. During this process, the landslide head with intact vegetation moved downward replacing bare landslide toes and leading to NDVI decrease at the lower part of the upper major scarp and NDVI increase at the upper part of the lower toes. NDVIs of gray-colored pixels (point 2 in Fig. 7) between the lower toes and upper major scarp of the landslide is stable, indicating the landslide head was intact as it moves down.

Based on NDVI time series, we analyzed inter-annual slope movement before the landslide occurred. We calculated annual maximum NDVI changes in 2016–2018 (Fig. 9a), NDVI changes in springs (Fig. 9b), summers (Fig. 9c) of 2016–2018, and changes in winters of 2015–2017 (Fig. 9d). From Fig. 9a, we can see that most monotonous decrease of annual maximum NDVI (red pixels) is found on the landslide surface. In particular, the signal of depressed vegetation was detected at the lower part of the upper major scarp (red pixels on black lines). There is also some NDVI decrease around the lower toes (red pixels around white lines). These NDVI decrease shows depressed vegetation signal as the landslide head moves down along the slope. Similar patterns on the landslide surface can be observed in the spring, summer and winter seasons (Fig. 9b–d). Monotonous NDVI increase can be found at the bottom of the landslide head (blue pixels on white lines, particularly in Fig. 9a, b), indicating

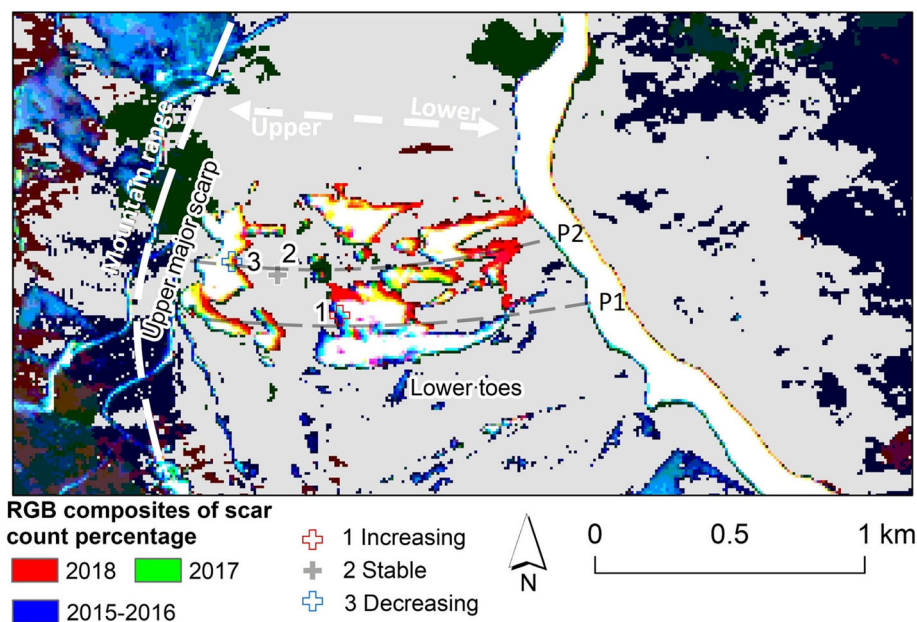


Fig. 7 RGB composite image of the landslide scar in three periods: 2015–2016, 2017, and 2018. Gray color has zero value in these three periods, and white color is consistently labeled as landslide scar (The Jinsha River is also in white color but can be easily excluded). Points 1, 2, and 3 are the three selected pixels with their NDVI time series analyzed in Fig. 8

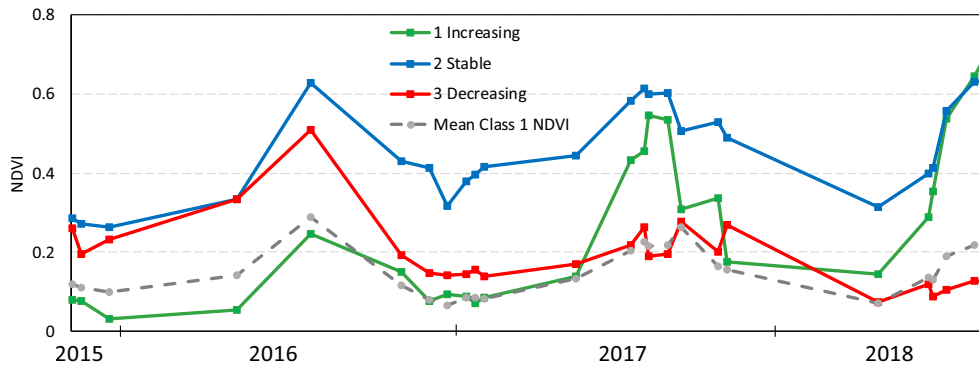


Fig. 8 Time series of three typical NDVI time series on the moving landslide surface. The typical decreasing NDVI pixel from the major scarp indicates the expansion of the landslide's main scarp. The typical increasing NDVI shows the downslope movement of the landslide body (These three time-series NDVI were derived from points in Fig. 7)

that the landslide head with intact vegetation cover moves downward replacing bare landslide toes. There are also some scattered pixels with monotonous increase/decrease of annual NDVI on other parts of the landslide surface, which probably indicates many fissures on the landslide head and their downslope movements.

There is some difference in NDVI decrease of different seasons (red pixels in Fig. 9b–d). Similar patterns of inter-annual NDVI

decrease were observed in springs and summers (red pixels in Fig. 9b, c) and fewer pixels with NDVI decrease was found for winters (red pixels in Fig. 9d). This result indicates that slope movement in the period of 2016–2018 (spring and summer change) is more severe than in 2015–2017, and significant slope displacement may occur from November 2017 to July 2018, the last year the slope fails.

Monotonous NDVI increase is widely distributed in the study area, the majority of which is located in vegetation consistent areas

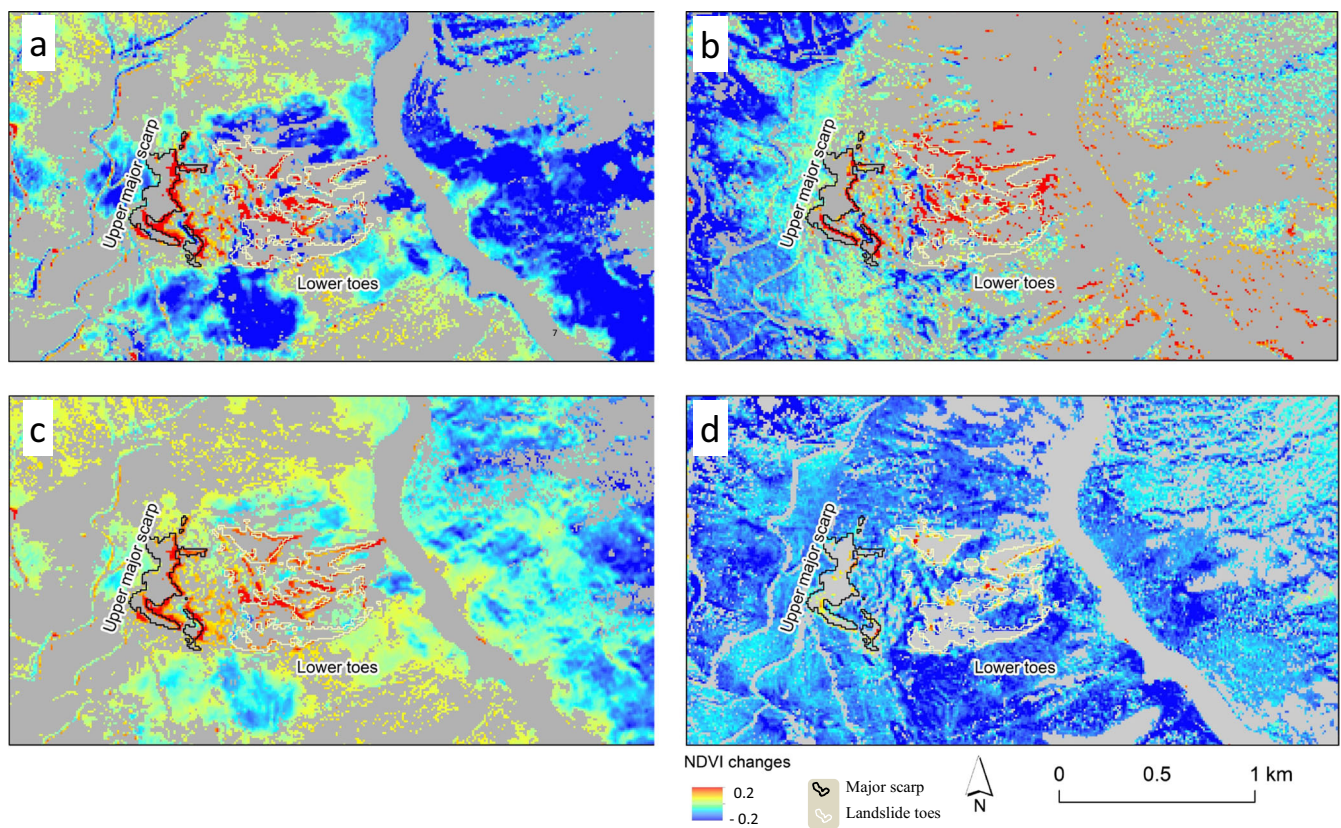


Fig. 9 Annual maximum NDVI difference in 2016–2018 (a) and inter-annual NDVI difference for springs in 2016–2018 (b), summers in 2016–2018 (c), winters in 2015–2017 (d). Take the annual maximum NDVI changes (a) as an example, positive values (red color) show continuous decrease of annual maximum NDVI in these 3 years (2016–2018) and negative values (blue color) show continuous increase from 2016 to 2018. Polygons of the landslide scarps (black polygons) and toes (white polygons) were extracted from Sentinel-2 image on 4 August 2017

unrelated to scarps and toes of the landslide. This is probably caused by clouds in some images (asterisk marked after date in Table 1) and natural vegetation fluctuation in different dates of images used for computation. For example, two out of three images used to calculate summer NDVI changes in 2016–2018 have clouds and the only summer image in 2016 has clouds, which directly leads to abnormal changes for both summer and annual maximum NDVI changes. In addition, there are 26 and 14 days' difference for calculating spring and winter NDVI changes and inter-annual vegetation conditions is probably different, which can also explain monotonous NDVI increase on non-landslide slopes.

Discussion

Capability of using Sentinel-2 to detect slope movement

Sentinel-2 is a recently launched global coverage, high spatial resolution (10 m in near-infrared, red, green, and blue bands), short revisit interval (5-day at the Equator) dataset. Although the spatial resolution of Sentinel-2 images is much coarser than sub-meter high optical images, such as WorldView or QuickBird images, it has much shorter revisit time and is cost-free. Despite these advantages rivals all others, its potential use in regional landslide hazard studies has been less explored (Lacroix et al. 2018). In this work, we proposed a method to use time series of Sentinel-2 optical images to capture slope displacement from November 2015 to August 2018 before the 10 October 2018 Jinsha River landslide. We first detected scarps and toes of the landslide by unsupervised classification. Then, slope movement was successfully detected before the landslide occur by examining changes of landslide scars and vegetation signals (NDVI). Our results were validated by using two high spatial resolution images in November 2015 and February 2018. This work demonstrated the potential of using Sentinel-2 time series data to detect slope displacement before landslides occur in large regions.

Compared with SAR technique, it is difficult for the 10 m resolution Sentinel-2 images to estimate slope displacement at a few centimeters. However, optical images such as Sentinel-2 have advantages to detect fast ground motions, which may pose problems in SAR techniques (Stumpf et al. 2017). For example, ground displacements of a few centimeters per day could render incoherence in SAR images (Wright 2002) but can be efficiently detected by our proposed method using Sentinel-2 images. In addition, the proposed Sentinel-2 algorithm is much easier than SAR techniques to detect slope movement. Vegetation signals are considered as noise and may lead to incoherence in SAR techniques, limiting their use in vegetation covered region. In contrast, our method uses changes in vegetation signal to detect slope displacement, and it can provide an ideal supplementary for SAR techniques over dense vegetation regions.

There is a lack of in situ measurements and sub-meter high spatial resolution images to estimate uncertainties in this work. Using two high spatial resolution images in 2015 and 2018, we validated extracted landslide scars from Sentinel-2 images. Omission errors in 2018 (25.1%) is likely caused by different acquisition date of Gaofen-2 (28 February 2018) and Sentinel-2 images (11 April 2018). However, those omissions occur on inactive parts of the landslide and extracted result of active

landslide parts are very accurate (e.g., lower boundary of the upper major scarp and boundaries of lower toes in Fig. 6). This result means that the proposed method is very sensitive to active parts of the landslide, even the slope movement is minor. This method may work well for slopes that caused vegetation to depress by releasing loose materials but have minor displacement. In addition, this method is easy to implement and sensible to slope movement for a large area. In this work, the proposed method only aims to detect slope movement, displacement estimation of the slope may be considered in future work.

Influence of clouds and vegetation phenology

In this work, we selected Sentinel-2 images with no clouds on the landslide surface. Clouds are major noises in optical remote sensing images and could severely affect image quality. To detect actual vegetation changes caused by landslides, pixels contaminated by clouds should be removed. Although preliminary cloud mask has been developed for Sentinel-2 dataset, its accuracy is still too low (Coluzzi et al. 2018). To monitor slope displacement over large regions, time series of Sentinel-2 images are needed, and reliable cloud masks are required. Therefore, robust algorithms should be developed to accurately detect clouds in Sentinel-2 images.

Another problem to use vegetation signals in optical images is the influence of vegetation phenology (Yang and Qi 2017), which is defined as the natural fluctuation of NDVI values in different seasons of a year (Fig. 10). Influenced by vegetation phenology, it is difficult to derive true NDVI changes caused by landslides by comparing vegetation signals of different seasons. To overcome phenology influence, we used different thresholds to extract landslide scars in the Sentinel-2 images and compared inter-annual vegetation signals (NDVI) of similar dates to derive slope movement. Because there are not enough Sentinel-2 observations in our work, we used annual maximum NDVI values and images of similar dates in three consecutive years to overcome the influence of vegetation phenology. In the future, as the Sentinel-2 platform operates regularly, dense and regular observations (5-day or less interval) would be possible to overcome phenology influence.

Despite we tried to minimize the influence of clouds and phenology in this work, some marked changes irrelevant to slope movement were also detected. Take the spring result (Fig. 9b) as an example, there are many marked changes colored blue, which means NDVI in 2016 is significantly lower than the value in 2018. This is because the image in 2016 was taken on 11 May, whereas image in 2018 was on 5 June. Because of vegetation phenology, vegetation in May–June experience dramatic increase in NDVI (Fig. 10) and normally NDVI values in May should be lower than that of June. The situation for the winter result (Fig. 9d) can also be explained by inter-annual vegetation phenology.

The result of summer can be explained by cloud contamination in Sentinel-2 images. From Sentinel-2 images (Fig. 11), we can see that clouds exist in 2016 (white clouds and dark shadows, Fig. 11b) and 2017 (little clouds, Fig. 11c). NDVI decrease (blue pixels) in summer result can be attributed to cloud contamination in 2016. Clouds and its shadows in 2016 image significantly lowered NDVI values, leading to marked changes on the opposite banks.

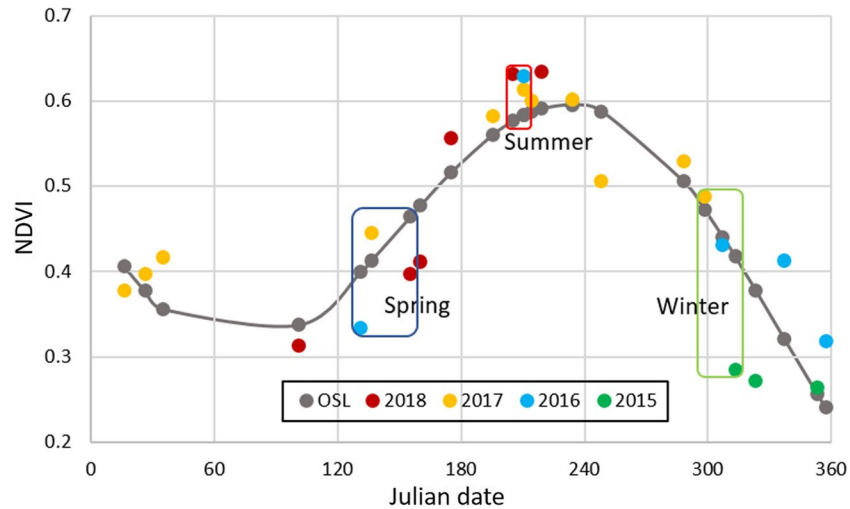


Fig. 10 Multi-year (Nov. 2015–Aug. 2018) cloud-free NDVI time series of the “Stable” pixel in Fig. 8. Solid black line is the ordinary least square (OLS) regression line (Zhu et al. 2014)

Other factors that may influence the result

This technique may be influenced by a few other factors, such as landslide size, climate, and terrain conditions. Limited by the 10 m spatial resolution of Sentinel-2, landslide scars smaller than a single 10 m × 10 m pixel cannot be detected. With this resolution, this technique is more efficient to monitor large landslides of similar sizes. If vegetation disturbed by slope movement recovers quicker than the observation cycle, it would be difficult for the technique to find slope movement. For example, in regions persistently covered by heavy clouds, snow, or other unfavorable conditions, valid observation intervals for the optical Sentinel-2 images would be much longer. If vegetation disturbed by slope movement during two valid observations

recovered to pre-disturbance level, this technique could fail. It is also possible that if the vegetation is much too dense (e.g., heavily forested terrains) that the signal of disturbed vegetation by slope movement may be obscured. In such case, the technique could not be applicable. It is also possible that if the displacement is very minor, the vegetation signal cannot be detected.

Although changes in vegetation species, land cover change, long-term vegetation changing trends, and other factors may cause signal changes in vegetation, their spatial and temporal patterns are different to changes caused by pre-landslide slope movement. Landslides are ground movements along the slope driven by gravity and the process is unique. Vegetation changes caused by slope movement are closely related to geomorphic features. For

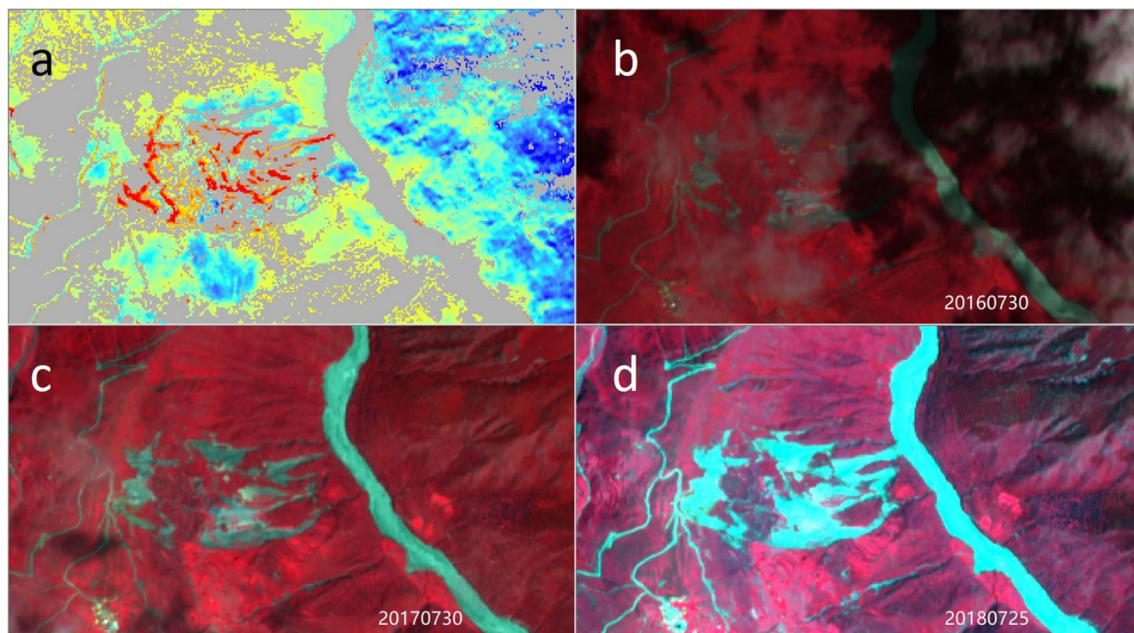


Fig. 11 Summer result of NDVI change (a), Sentinel-2 image on 30 July 2016 (b), on 30 July 2017 (c), and on 25 July 2018, respectively

example, near the landslide crown, vegetation will get sparser (decrease of NDVI), when tensions cracks get larger. As the slope moves down, affected vegetation (not necessarily mortality) should display changes related to this geomorphic process. They are different in the flowing points: (1) pre-landslide features are site-specific, vegetation disturbances are probably constrained on a single slope, whereas other disturbances are widespread phenomenon; (2) slope movement is controlled by topography, but the other vegetation disturbance is not closely related to terrain characteristics (Yang et al. 2017).

Despite this work did not estimate moving rate of the landslide before failure, it has the potential to estimate slope movement by decomposing sub-pixels. As more Sentinel-2 images become available in a single year, we can use dense observations to model annual mathematical NDVI curves (as shown in Fig. 10). Based on those NDVI models, it is possible to estimate sub-pixel slope movement by decomposing Sentinel-2 pixels using all available images of the year (Deng and Zhu 2018). Therefore, more efforts are needed to fully exploit this time series optical data in detecting slope displacement at a regional scale.

Conclusion

In this work, we explored the potential use of time series Sentinel-2 data in detecting slope movement before the occurrence of the Jinsha River landslide in October 2018. Based on this dataset, we developed a simple but effective method to detect slope movement using changes of vegetation signals. This method is easy to perform and sensitive to vegetation changes caused by slope displacement. Using the 10 m spatial resolution Sentinel-2 images, slope movement in 2015–2018 was detected before the landslide occurred. Different from SAR and very high-resolution optical techniques, the proposed method favors rough mountain terrains covered by vegetation.

By exploiting its high temporal resolution, slope displacement was found more severe in the last year before the slope fail (since November 2017). At full load, Sentinel-2 data have high spatial and temporal resolution (10 m in near-infrared, red, green, and blue bands, 5-day revisit interval at the Equator) and is cost-free. In the future, with the platform continues working, more data will be accumulated and time series of a year with 5-day interval or high can be achieved. Well-registered optical time-series images have the capability to detect pre-landslide slope movement in large regions. This dataset should be fully exploited in the landslide community, and we call for more use of such time consistent, cost-free datasets in future for landslide risk reduction studies.

Acknowledgments

This work was supported by the National Science Foundation of China (NO. 41807500) and the National Key Research and Development Program of China (NO. 2017YFC1503000). We show gratitude to following MSc students: Jianghua Liao, Zhen Zhang, Yuhong Ma, and Lijuan Wang for their help in collecting some of the basic information for the Jinsha River landslide at the initial stage of this work. We also express our thanks to Prof. Qiang Xu and Dr. Weile Li from the Stake Key Laboratory of Geo-hazards for generously sharing Ziyuan-3 and Gaofen-2 high spatial resolution images in 2015 and 2018. Contributions by editor and reviewers of this work are also deeply appreciated.

References

- Baidu (2018) <http://baike.baidu.com/item/金沙江堰塞湖/22921677?fr=aladdin>. Accessed on 02 March 2019
- Coluzzi R, Imbrenda V, Lanfredi M, Simoniello T (2018) A first assessment of the Sentinel-2 level 1-c cloud mask product to support informed surface analyses. *Remote Sens Environ* 217:426–443. <https://doi.org/10.1016/j.rse.2018.08.009>
- Deng C, Zhu Z (2018) Continuous subpixel monitoring of urban impervious surface using Landsat time series. *Remote Sens Environ*. <https://doi.org/10.1016/j.rse.2018.10.011>
- Elhag M, Alshamsi D (2019) Integration of remote sensing and geographic information systems for geological fault detection on the island of Crete, Greece. *Geosci Instrum Method Data Syst* 8:45–54. <https://doi.org/10.5194/gi-8-45-2019>
- Fan X, Xu Q, Scaringi G, Dai L, Li W, Dong X, Zhu X, Pei X, Dai K, Havenith H-B (2017) Failure mechanism and kinematics of the deadly June 24th 2017 Xinmo landslide, Maoxian, Sichuan, China. *Landslides* 14:2129–2146. <https://doi.org/10.1007/s10346-017-0907-7>
- Fan X, Xu Q, Alonso-Rodriguez A, Subramanian S, Li W, Zheng G, Dong X, Huang R (2019) Successive landsliding and damming of the Jinsha River in eastern Tibet, China: prime investigation, early warning, and emergency response. *Landslides* 1–8. <https://doi.org/10.1007/s10346-019-01159-x>
- Fiorucci F, Ardizzone F, Mondini AC, Viero A, Guzzetti F (2018) Visual interpretation of stereoscopic NDVI satellite images to map rainfall-induced landslides. *Landslides* 16:165–174. <https://doi.org/10.1007/s10346-018-1069-y>
- Gascon F, Bouzinac C, Thépaut O, Jung M, Francesconi B, Louis J, Lonjou V, Lafrance B, Massera S, Gaudel-Vacaresse A, Languille F, Alhammoud B, Viallefond F, Pflug B, Bieniarz J, Clerc S, Pessiot L, Trémas T, Cadau E, De Bonis R, Isola C, Martimort P, Fernandez V (2017) Copernicus sentinel-2A calibration and products validation status. *Remote Sens* 9:584
- Igwe O (2018) The characteristics and mechanisms of the recent catastrophic landslides in Africa under IPL and WCOE projects. *Landslides* 15:2509–2519. <https://doi.org/10.1007/s10346-018-1064-3>
- Intrieri E, Raspini F, Fumagalli A, Lu P, Del Conte S, Farina P, Allievi J, Ferretti A, Casagli N (2018) The Maoxian landslide as seen from space: detecting precursors of failure with Sentinel-1 data. *Landslides* 15:123–133. <https://doi.org/10.1007/s10346-017-0915-7>
- Lacroix P, Berthier E, Maquerhua ET (2015) Earthquake-driven acceleration of slow-moving landslides in the Colca valley, Peru, detected from Pléiades images. *Remote Sens Environ* 165:148–158. <https://doi.org/10.1016/j.rse.2015.05.010>
- Lacroix P, Bièvre G, Pathier E, Knies U, Jongmans D (2018) Use of Sentinel-2 images for the detection of precursory motions before landslide failures. *Remote Sens Environ* 215:507–516. <https://doi.org/10.1016/j.rse.2018.03.042>
- Leprince S, Barbot S, Ayoub F, Avouac JP (2007) Automatic and precise orthorectification, coregistration, and subpixel correlation of satellite images, application to ground deformation measurements. *IEEE Trans Geosci Remote Sens* 45:1529–1558. <https://doi.org/10.1109/TGRS.2006.888937>
- Lu P, Casagli N, Catani F, Tofani V (2012) Persistent scatterers interferometry hotspot and cluster analysis (psi-hca) for detection of extremely slow-moving landslides. *Int J Remote Sens* 33:466–489. <https://doi.org/10.1080/01431161.2010.536185>
- Notti D, Giordan D, Calo F, Pepe A, Zucca F, Galve JP (2018) Potential and limitations of open satellite data for flood mapping. *Remote Sens* 10:1673. <https://doi.org/10.3390/rs10111673>
- Sanchez YS, Martinez-Grana A, Frances FS, Picado MM (2018) Mapping wildfire ignition probability using sentinel 2 and LiDAR (Jerte Valley, Caceres, Spain). *Sensors* 18:826. <https://doi.org/10.3390/s18030826>
- Stumpf A, Malet J-P, Delacourt C (2017) Correlation of satellite image time-series for the detection and monitoring of slow-moving landslides. *Remote Sens Environ* 189:40–55. <https://doi.org/10.1016/j.rse.2016.11.007>
- Tomás R, Li Z, Lopez-Sanchez JM, Liu P, Singleton A (2016) Using wavelet tools to analyse seasonal variations from InSAR time-series data: a case study of the Huangtupo landslide. *Landslides* 13:437–450. <https://doi.org/10.1007/s10346-015-0589-y>
- Wasowski J, Bovenga F (2014) Investigating landslides and unstable slopes with satellite multi temporal interferometry: current issues and future perspectives. *Eng Geol* 174:103–138. <https://doi.org/10.1016/j.enggeo.2014.03.003>
- Wright TJ (2002) Remote monitoring of the earthquake cycle using satellite radar interferometry. *Philos Trans A Math Phys Eng Sci* 360:2873–2888
- Xinhua N (2018a) http://www.xinhuanet.com/english/2018-11/15/c_137609161.htm. Accessed on 16 December 2018
- Xinhua N (2018b) http://tibet.news.cn/2018-10/14/c_137531836.htm. Accessed on 02 March 2019

- Xu Q, Zheng G, Li W, He C, Dong X, Guo C, Feng W (2018) Study on successive landslide damming events of Jinsha River in Baige village on October 11 and November 3, 2018. *J Eng Geol* 26:1534–1551. <https://doi.org/10.13544/j.cnki.jeg.2018-406>
- Yang W, Qi W (2017) Spatial-temporal dynamic monitoring of vegetation recovery after the Wenchuan earthquake. *IEEE J Sel Top Appl Earth Observ Remote Sens* 10:868–876. <https://doi.org/10.1109/jstars.2016.2616511>
- Yang W, Wang M, Shi P (2013) Using modes ndvi time series to identify geographic patterns of landslides in vegetated regions. *IEEE Geosci Remote Sens Lett* 10:707–710
- Yang W, Qi W, Wang M, Zhang J, Zhang Y (2017) Spatial and temporal analyses of post-seismic landslide changes near the epicentre of the Wenchuan earthquake. *Geomorphology* 276:8–15. <https://doi.org/10.1016/j.geomorph.2016.10.010>
- Zhang X, Wang M, Liu K, Xie J, Xu H (2018) Using NDVI time series to diagnose vegetation recovery after major earthquake based on dynamic time warping and lower bound distance. *Ecol Indic* 94:52–61. <https://doi.org/10.1016/j.ecolind.2018.06.026>
- Zhu Z, Woodcock CE (2014) Continuous change detection and classification of land cover using all available Landsat data. *Remote Sens Environ* 144:152–171. <https://doi.org/10.1016/j.rse.2014.01.011>
- Zhu X, Helmer EH (2018) An automatic method for screening clouds and cloud shadows in optical satellite image time series in cloudy regions. *Remote Sens Environ* 214:135–153. <https://doi.org/10.1016/j.rse.2018.05.024>

W. Yang (✉) · **Y. Wang** (✉) · **Y. Wang** · **C. Ma**

Jinyun Forest Ecosystem Research Station, School of Soil and Water Conservation, Beijing Forestry University, Beijing, 100083, China
Email: yang_wentao@bjfu.edu.cn
Email: wangyunqi@bjfu.edu.cn

S. Sun

National Climate Center, China Meteorological Administration, Beijing, 100081, China